34th Annual International Conference of the IEEE EMBS
San Diego, California USA, 28 August - 1 September, 2012

Material depth reconstruction method of multi-energy X-ray images using neural network

Woo-Jin Lee[1], Dae-Seung Kim[1], Sung-Won Kang[1], Won-Jin Yi[2]

Abstract— **With the advent of technology, multi-energy X-ray imaging is promising technique that can reduce the patient's dose and provide functional imaging. Two-dimensional photon-counting detector to provide multi-energy imaging is under development. In this work, we present a material decomposition method using multi-energy images. To acquire multi-energy images, Monte Carlo simulation was performed. The X-ray spectrum was modeled and ripple effect was considered. Using the dissimilar characteristics in energy-dependent X-ray attenuation of each material, multiple energy X-ray images were decomposed into material depth images. Feedforward neural network was used to fit multi-energy images to material depth images. In order to use the neural network, step wedge phantom images were used for training neuron. Finally, neural network decomposed multi-energy X-ray images into material depth image. To demonstrate the concept of this method, we applied it to simulated images of a 3D head phantom. The results show that neural network method performed effectively material depth reconstruction.**

I. Introduction

Conventional X-ray image has difficulty in discriminating material due to overlapped objects and necessity of reducing patient's dose [1]. Recently, various methods are developed to reduce the patient's dose and to improve diagnosis of disease. One of the approaches is to acquire multi-energy X-ray images and apply them to material differentiation.

In order to acquire multi-energy X-ray images, several techniques such as dual source CT, sandwich detector, or photon-counting detector have been utilized. However, these methods provide limited number of energy bins and energy resolution is low. Thus, if dual or triple energy is only used to acquire images, the number of images that can distinguish the materials might be reduced. In addition, multi-energy in various energy bands might be hardly acquired. Similar to dual source CT, sandwich detector also has low energy resolution.

By the way, among these methods, photon counting method provides several advantages; the most radiation-efficient, low-dose, and multi energy X-ray detecting. Due to the usefulness of photon counting detector, this method has been conducted by many researchers [2-5].

As the previous researchers have shown, multi-energy can support to distinguish the materials due to atomic reacting to various energy domains. Specifically, functional imaging that represents the characteristics of material component, not simply X-ray attenuation images, is feasible by using multi-energy X-ray images. In addition, high Contrast-to-Noise Ratio can be acquired with equal radiation dose.

According to previous researches, several studies have been conducted by using dual-energy [6-8] or triple-energy [9] to discriminate materials. These researches used pseudo inverse matrix to decompose material. But they supposed that X-ray reacting is linear with limited number of energy bin.

In order to overcome this problem, cubic equation has been applied [10], or a geometrical constraint [11] has been set. Despite using cubic equation, however, its application and modeling the non-linear relation might be complicated as the number of energy bin increases. On the other hand, artificial neural networks can predict the non-linear relationship better than other methods [12-14].

As we, writers and co-workers, have been developing photon-counting detector, we simulated the multi-energy X-ray images using Monte Carlo simulation in advance. The simulated images resulting from step wedge phantom were used to train neuron. After that, simulated multi-energy images of real patient's phantom were decomposed into material depth image by using artificial neural network.

II. Materials and Methods

A. Multi-energy image simulation

Multi-energy image was acquired by penMesh Monte Carlo simulation [15] based on PENELOPE. Figure 1 shows experimental simulation geometry. X-ray source was positioned at z-axis and the direction was toward –z with semi aperture angle of 4.62 degree. The number of photon histories was 2×10^{10}. Tally to produce radiographic images was activated and image was produced by scoring the 2D energy deposition distribution inside the detector. Unit was eV/cm^2 per history. Detector size was 6 cm × 6 cm × 0.06 cm and pixel number was 200 × 200.

*This work was supported by the Industrial Strategic Technology Development Program (10038695) funded by the Ministry of Knowledge Economy (MKE, Korea).

[1]Interdisciplinary Program in Radiation Applied Life Science major, College of Medicine, BK21, and Dental Research Institute, Seoul National University, South Korea

[2]Department of Oral and Maxillofacial Radiology, BK21, and Dental Research Institute, School of Dentistry, Seoul National University, South Korea

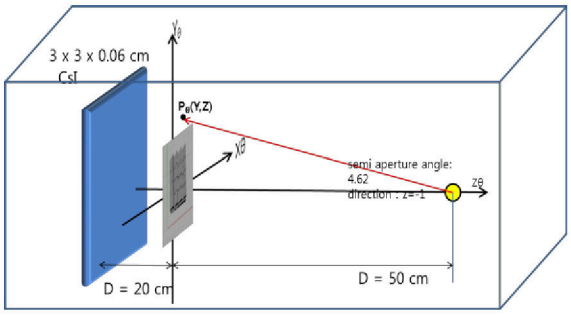

Figure 1. Image acquisition geometry

The polychromatic X-ray spectrum was shown in Figure 2. The range of spectrum was from 20 keV to 120 keV with tungsten anode. As illustrated in Figure 2, the ripple effect was simulated [16] and 20 % of ripple effect was applied. In order to obtain practical result, the assumption was established; although detector can discriminate each energy bin, energy response rate is imperfect. Based on this hypothesis, the energy response rate was modeled (Fig. 3).

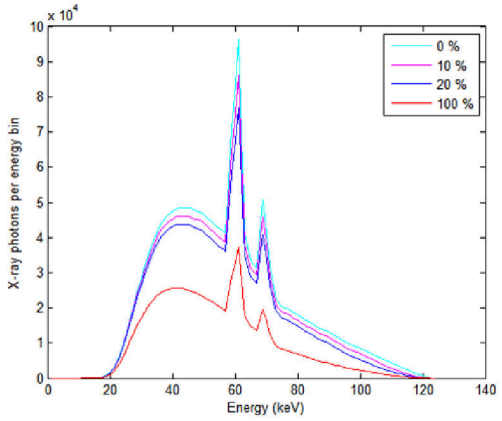

Figure 2. X-ray spectrum simulation. The ripple effect was considered from 0 to 100 percent.

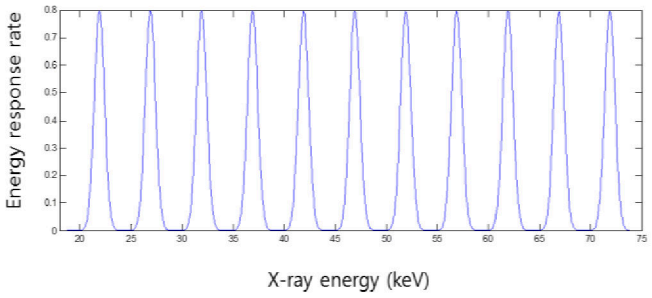

Figure 3. Detector response function was designed. The energy resolution was 1.18 keV in FWHM for each bin.

As seen in Figure 3, the energy response resolution was 1.18 keV in FWHM for each bin. Total 11 energy bin was used and mean energy was increased 5 keV per each bin, from 21.9 keV to 71.9 keV. Consequentially, the image acquired through the simulation was non-linear relationship to each energy bin.

B. Virtual Phantom generation

In Figure 4, virtual step wedge phantom was created to make training data. Bone tissue, cancer tissue, and normal soft tissue were arranged from the bottom. Each material has 4 steps; thus, 64 depth cases were created. For a test on realistic data, the real patient's CT data was segmented and consisted of these three kinds of tissues (Fig. 5). The cancer tissue was positioned in the maxillary sinus area. Each materials attenuation coefficient was based on ICRP Publication 110.

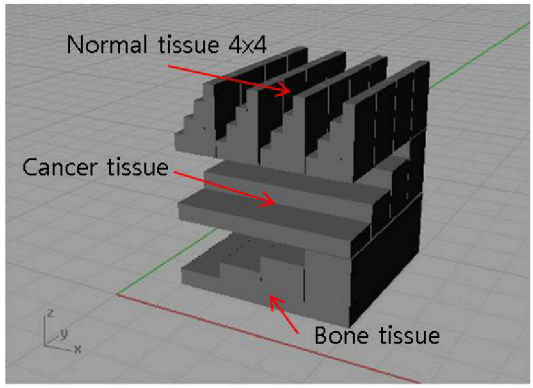

Figure 4. Step wedge phantom for training neural network

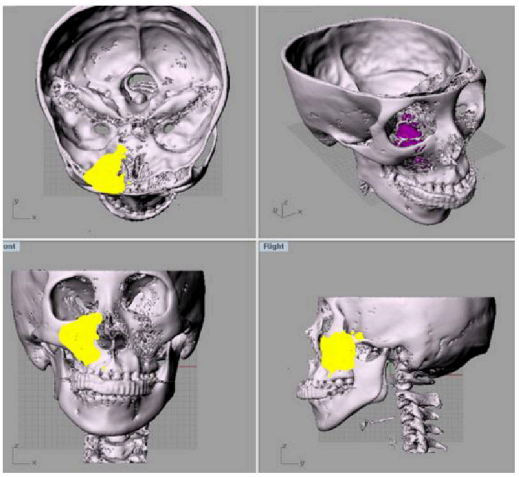

Figure 5. Three-dimensional human head phantom. Cancerous tissue was fabricated and position in maxillary sinus.

C. Neural network based decomposition algorithm

The non-linear relationship between each energy bin and material depth can be resolved by feedforward neural network. Each image obtained from each 11 energy bin was set in the input node, and the number of neurons of hidden layer was set into 40. Output nodes represented each material depth. First of all, the weight of hidden layers was trained based on each material depth of energy bin data. The Levenberg-Marquardt algorithm [17] was used to calculate optimal weighting factor. A performance function was mean squared error. Training cases of 2816(64 depth cases × 11 energy bins × 4 neighborhoods) were used. After finishing the training process, the experimental data was entered into the input nodes. The

projection of 3D head phantom was generated from Monte Carlo simulation in each energy bin. Then, simulated each energy bin image was entered into the input nodes and decomposed as bone tissue, cancer tissue, and normal tissue, respectively.

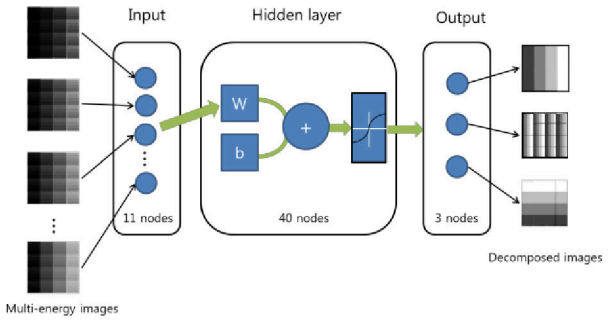

Figure 6. Feedforward neural network. Each energy bin data was set in the input nodes and it decomposed as trained material depth value.

III. Results

Figure 7 shows simulated images for input nodes of neural networks.

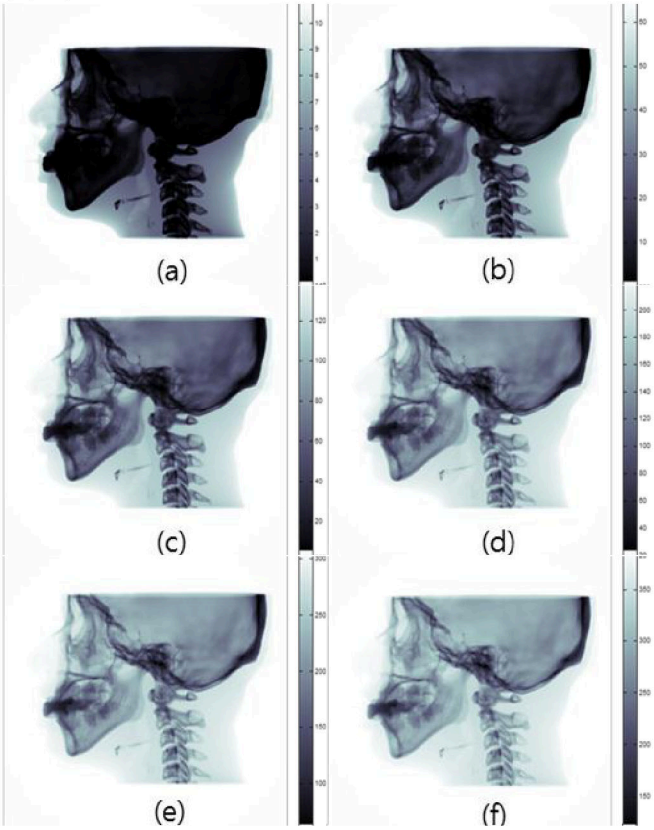

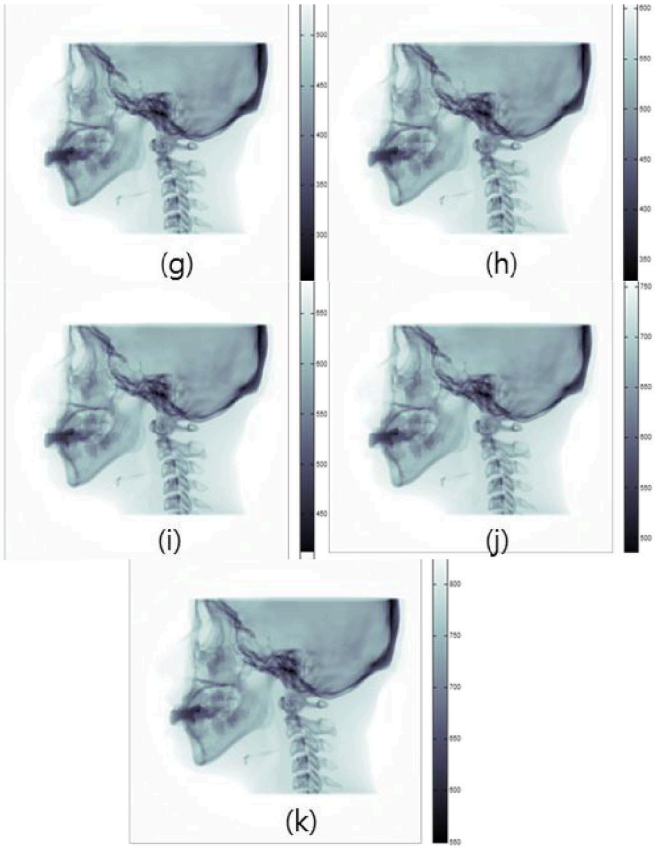

Figure 7. Simulated results of each energy bin data. (a)-(k) multi-energy image images (from 21.9 keV to 71.9 keV, respectively).

The trained neural network decomposed each energy bin images into each material depth image. In the projected images, it was impossible to discern between cancer tissue and normal tissue. On the other hand, in the decomposed image, cancer tissue and normal tissue were clearly distinguished between them. Figure 8 shows material depth images of cancer (Fig. 8(a)), bone (Fig. 8(b)), and normal tissue (Fig. 8(c)) in unit of cm. The accuracy was measured in the region of maxillary sinus. The difference rate of each material was 1.2% for bone, 2.3% for cancer tissue and 5.2% for normal tissue.

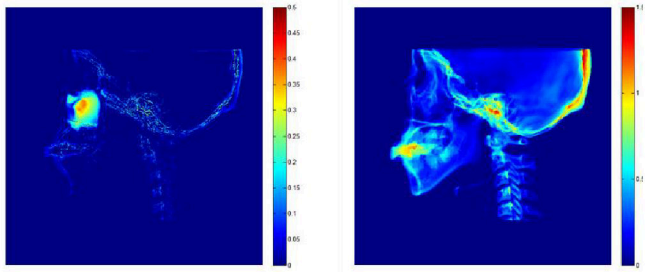

(a) (b)

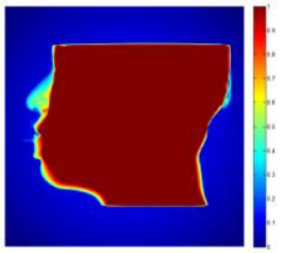

(c)

Figure 8. Depth reconstruction of each material. Bone tissue, cancer tissue and normal tissue depth was reconstructed.

IV. CONCLUSION

Each separated X-ray image was not able to discriminate the cancer tissue; but, overlapped images were decomposed into material depth images. The intrinsic characteristics of the neural network approach seem to yield the suitable results. Findings from this study suggest that feedforward neural networks were effective tools for approximation of non-linear system. Beneficial as it may be, it was complicated to divide various materials because of intricate training process. For further research, it is recommended that various materials and energy bin should be tested to obtain more robust results. Given the energy-discrimination property, we assume that feedforward neural network can be the effective tool for the precise measurement of tissue properties in the field of diagnosis.

REFERENCES

[1] M. Firsching, *et al.*, "Material resolving X-ray imaging using spectrum reconstruction with Medipix2," *Nuclear Instruments & Methods in Physics Research Section a-Accelerators Spectrometers Detectors and Associated Equipment,* vol. 591, pp. 19-23, Jun 11 2008.

[2] G. A. Howland, *et al.*, "Photon-counting compressive sensing laser radar for 3D imaging," *Applied Optics,* vol. 50, pp. 5917-5920, Nov 1 2011.

[3] Y. Ihara, *et al.*, "Development of photon counting system with FPGA for precise measurement of radiophotoluminescence," *Radiation Measurements,* vol. 46, pp. 1574-1577, Dec 2011.

[4] X. Wang, *et al.*, "MicroCT with energy-resolved photon-counting detectors," *Phys Med Biol,* vol. 56, pp. 2791-816, May 7 2011.

[5] X. Wang, *et al.*, "Material separation in x-ray CT with energy resolved photon-counting detectors," *Medical Physics,* vol. 38, pp. 1534-46, Mar 2011.

[6] X. W. Wang, *et al.*, "Material discrimination by high-energy x-ray dual-energy imaging," *High Energy Physics and Nuclear Physics-Chinese Edition,* vol. 31, pp. 1076-1081, Nov 2007.

[7] K. V. Haderslev and M. Staun, "Comparison of dual-energy X-ray absorptiometry to four other methods to determine body composition in underweight patients with chronic gastrointestinal disease," *Metabolism,* vol. 49, pp. 360-6, Mar 2000.

[8] K. L. Goh, *et al.*, "Correction of energy-dependent systematic errors in dual-energy x-ray CT using a basis material coefficients transformation method," *Ieee Transactions on Nuclear Science,* vol. 44, pp. 2419-2424, Dec 1997.

[9] M. Firsching, *et al.*, "Multi-energy X-ray imaging as a quantitative method for materials characterization," *Adv Mater,* vol. 23, pp. 2655-6, Jun 17 2011.

[10] J. M. Letang, *et al.*, "Signal-to-noise ratio criterion for the optimization of dual-energy acquisition using virtual x-ray imaging: application to glass wool," *Journal of Electronic Imaging,* vol. 13, pp. 436-449, Jul 2004.

[11] S. N. Le, *et al.*, "Volumetric reconstruction from multi-energy single-view radiography," in *Computer Vision and Pattern Recognition, 2008. CVPR 2008. IEEE Conference on*, 2008, pp. 1-8.

[12] I. V. Tetko, *et al.*, "Polynomial neural network for linear and non-linear model selection in quantitative-structure activity relationship studies on the internet," *SAR QSAR Environ Res,* vol. 11, pp. 263-80, 2000.

[13] J. H. Jiang, *et al.*, "Neural network learning to non-linear principal component analysis," *Analytica Chimica Acta,* vol. 336, pp. 209-222, Dec 30 1996.

[14] S. Cincotti, *et al.*, "A neural network model of parametric non-linear hysteretic inductors," *Ieee Transactions on Magnetics,* vol. 34, pp. 3040-3043, Sep 1998.

[15] A. Badal, *et al.*, "penMesh-Monte Carlo Radiation Transport Simulation in a Triangle Mesh Geometry," *Ieee Transactions on Medical Imaging,* vol. 28, pp. 1894-1901, Dec 2009.

[16] M. Matsumoto, *et al.*, "Effects of voltage ripple and current mode on diagnostic x-ray spectra and exposures," *Medical Physics,* vol. 18, pp. 921-7, Sep-Oct 1991.

[17] G. Lera and M. Pinzolas, "Neighborhood based Levenberg-Marquardt algorithm for neural network training," *IEEE Trans Neural Netw,* vol. 13, pp. 1200-3, 2002.